ARTICLE

Journal of Materials Chemistry
www.rsc.org/materials

Ethylene glycol-mediated synthesis of metal oxide nanowires

Xuchuan Jiang,[a] Yuliang Wang,[a] Thurston Herricks[b] and Younan Xia*[a]

[a]*Department of Chemistry, University of Washington, Seattle, Washington 98195, USA. E-mail: xia@chem.washington.edu*
[b]*Department of Materials and Engineering, University of Washington, Seattle, Washington 98195, USA*

Received 3rd November 2003, Accepted 10th December 2003
First published as an Advance Article on the web 21st January 2004

A simple and convenient method has been demonstrated for large-scale synthesis of metal oxide (including TiO_2, SnO_2, In_2O_3, and PbO) nanowires with diameters around 50 nm and lengths up to 30 μm. In a typical procedure, tetraalkoxyltitanium, $Ti(OR)_4$ (with R = $-C_2H_5$, *–iso*-C_3H_7, or *–n*-C_4H_9), was added to ethylene glycol and heated to 170 °C for 2 h under vigorous stirring. The alkoxide was transformed into a chain-like, glycolate complex that subsequently crystallized into uniform nanowires. Similarly, nanowires made of tin glycolate were synthesized by refluxing $SnC_2O_4{\cdot}2H_2O$ in ethylene glycol at 195 °C for 2 h, and nanowires consisting of indium and lead glycolates were prepared by adding $In(OOCC_7H_{15})(O^iPr)_2$ and $Pb(CH_3COO)_2$ to ethylene glycol, followed by heating at 170 °C for 2 h. The nanowires could be readily collected as precipitates after the reaction solutions had been cooled down to room temperature. By calcining at elevated temperatures, each glycolate precursor could be transformed into the corresponding metal oxide without changing the wire-like morphology. Electron microscopic and XRD powder diffraction studies were used to characterize the morphology, crystallinity, and structure of these nanowires before and after calcination at various temperatures. A plausible mechanism was also proposed to account for the one-dimensional growth of such nanostructures in a highly isotropic medium. This mechanism was supported by XRD, FT-IR, solid state ^{13}C-NMR, and TGA measurements. As a demonstration of potential applications, the polycrystalline nanowires made of SnO_2 were used as functional components to fabricate sensors that could detect combustible gases (CO and H_2) with greatly enhanced sensitivity under ambient conditions.

I. Introduction

One-dimensional (1D) nanostructures (such as rods, wires, whiskers, belts, and tubes) represent a class of intriguing nanostructured materials to study because of their unique electronic, optical, and magnetic properties.[1] Among all approaches to 1D nanostructures, the simplest is probably the one that involves the use of anisotropy in crystal structure as the confinement. When a solid is composed of building blocks with chain-like conformations, it always tends to grow into 1D structures as directed and confined by the anisotropic interactions between building blocks. This notion is supported by many examples. For instance, a number of inorganic minerals such as asbestos and chrysolite are well-known to exhibit a habit for fibrous growth,[2] which is mainly determined by the chain structures, or some other anisotropic arrangements between ions or ionic groups in their crystal lattices. For poly(sulfur nitride), or $(SN)_x$, uniform nanowires could be readily grown from the vapor phase with diameters as thin as 20 nm and lengths up to hundreds of micrometers.[3] In addition, $M_2Mo_6X_6$ (M = Li, Na; X = Se, Te) have been readily synthesized as nanowire bundles of ~1 μm in diameter and up to ~20 μm in length because their structures are characterized by close packing of linear chains in the formula of $[Mo_6X_6]^{2-}$.[4] Most recently, trigonal phase Se and Te have been demonstrated as a class of solids that can be easily grown as various types of 1D nanostructures.[5] For these two solids, both of them contain helical chains that are packed into hexagonal lattices through van der Waals interactions. As a result, crystal growth occurs predominantly along the axial direction of helical chains, favoring the stronger covalent bonding within each chain over the relatively weaker van der Waals forces among the chains. As a unique feature associated with these two materials, they could be readily produced as nanowires with uniform diameters, which are essentially the same as the dimensions of the seeds perpendicular to the growth direction.

The potential of this method is, however, greatly limited by the requirement that the solid material to be synthesized as 1D nanostructures must crystallize in a highly anisotropic (in most cases, chain-like) conformation. Here we demonstrate that this approach can be extended to directly process a number of metal oxides (*e.g.* TiO_2, SnO_2, In_2O_3, and PbO) into nanowires despite their more or less isotropic crystal structures. The key modification to the procedure is the formation of a chain-like precursor by refluxing a suitable metal salt in ethylene glycol.[6] As induced and directed by highly anisotropic interactions, the chain-like species spontaneously aggregate into nanowires with uniform diameters. When calcined in air, the glycolate precursors can be converted to metal oxides with controllable compositions and phase structures while maintaining the wire-like morphology. Different from single crystalline nanowires (and belts) of oxide ceramics previously synthesized using gas-phase routes,[7] the nanowires described here were polycrystalline in structure (with a typical grain size in the range of 5 to 20 nm) and thus intrinsically larger surface areas.

Ethylene glycol has been widely used in the so-called polyol synthesis of metal (both pure and alloyed) nanoparticles due to its strong reducing power and relatively high boiling point (~197 °C).[8] It has also been explored as a cross-linking reagent in sol-gel processing to facilitate the formation of crack-free films.[9] Recently, Kriven and co-workers have synthesized $BaTiO_3$ and Ba_2TiO_4 powders through a route that involved complexation with ethylene glycol, followed by polymerization.[10] Kakihana and co-workers have also prepared $LaMnO_{3+d}$ powders *via in situ* polyesterification between ethylene glycol and citric acid, followed by calcination at an

DOI: 10.1039/b313938g

elevated temperature.[11] In addition, ethylene glycol has been used to fabricate mesostructures of titania, tin dioxide, zirconia, and niobium oxide by forming glycolate precursors because of its coordination ability with transition metal ions.[12] It is worth pointing out that the products of all these polyol-mediated syntheses were either nanoparticles or micrometer-sized powders. To our knowledge, the work described here represents the first demonstration that 1D nanostructures of various metal oxides could be readily synthesized using a polyol-mediated process. In addition to the metal oxides discussed in this paper, it is believed that this approach is a generic one, and should be extendable to cover all major classes of oxide-based ceramics.

II. Experimental

Chemicals and materials

Titanium(IV) tetraethoxide (technical grade), titanium(IV) tetraisopropoxide (97%), titanium(IV) tetrabutoxide (97%), tin(II) oxalate and lead(II) acetate were all purchased from Aldrich. $In(OOCC_7H_{15})(O^iPr)_2$ was obtained as a solution in isopropanol (5 g/100 mL) from Chemat Technology (Northridge, CA). Ethylene glycol (EG, Certified, Fisher) was bought from Fisher. All chemicals were used as-received. Polished silicon wafers (test grade, n-doped) were obtained from Silicon Sense (Nashua, NH). Carbon-coated copper grids for holding TEM samples were purchased from Ted Pella (Cat. No. 01801, Redding, CA).

Synthesis of metal glycolate nanowires

Titanium glycolate nanowires with uniform diameters were synthesized by heating a solution of titanium(IV) alkoxide in EG at 170 °C for 2 h. In a typical synthesis, 0.050 mL (~0.147 mmol) titanium(IV) butoxide was added to a 50-mL flask that contained 10 mL EG, with all operations being performed inside a glove box purged with nitrogen gas. The solution was then taken out from the glove box and heated to 170 °C using an oil bath under magnetic stirring for 2 h. After cooling down to room temperature, the white flocculate was harvested using centrifugation, followed by washing with de-ionized water and ethanol several times to remove excess EG from the sample. The precipitate was finally dried in a vacuum oven at 50 °C for 4 h and used for further characterization. Other titanium(IV) alkoxides, $Ti(OR)_4$ (R = $-C_2H_5$ and *–iso*-C_3H_7) could also serve as precursors for the synthesis of titanium glycolate nanowires. Once collected, the glycolate nanowires were directly placed in a box oven and calcined into the amorphous (at 350 °C), anatase (at 500 °C) and rutile (at 850 °C) phases of TiO_2 in air. We have also examined several other solvents (all from Aldrich) such as di-ethylene glycol (99%), tri-ethylene glycol (99%), and tetra-ethylene glycol (99%). Wire-like nanostructures could still be obtained but none of the samples was uniform in size.

Similarly, nanowires made of tin(II), indium(III) and lead(II) glycolates were synthesized by adding $SnC_2O_4{\cdot}2H_2O$, $In(OOCC_7H_{15})(OC_3H_7)_2$ or $Pb(CH_3COO)_2$ to EG and heating for 2 h at 195, 170, and 170 °C, respectively. After the solutions had been cooled down, nanowires with uniform diameters around 50 nm and lengths up to tens of micrometers could be collected as white precipitates by centrifugation. These nanowires composed of metal glycolates could be subsequently converted to SnO_2 or In_2O_3 by calcining at 500 °C for 2 h, and PbO by calcining at 600 °C for 4 h without changing their wire-like morphology.

Fabrication of sensors based on SnO_2 nanowires

In a typical procedure, two gold electrodes (with a separation of 100 μm) were fabricated by first sputtering a thin layer of chromium (~30 nm), followed by another layer of gold (~150 nm) onto a masked glass substrate. The precursor nanowires were then cast as a thin film (~5 × 5 × 0.5 mm^3) spanning across the two electrodes by using a mixture of the as-synthesized white precipitate and ethanol. After calcination in air at 500 °C for 1 h, copper wires were connected to the gold electrodes with silver paste. All results shown in this paper were obtained from the same sensor, which was hosted in a closed plastic tube (~50 mL in size) equipped with appropriate inlets and outlets for gas flow. The two copper wires coming out of the host tube were connected to a Keithley 236 sourcemeter, which served as both voltage source and current reader. The pristine sensor (in air) was found to exhibit the typical behavior of a varistor, exhibiting an exponential decay in resistance as the voltage was ramped up. For consistency, a potential of 10 V was applied across the two gold electrodes for all measurements, and the air coming from an ordinary fume hood was used as the background gas. Under these conditions, the resistance of a typical sensor was located in the range of 5 to 10 GΩ.

Instrumentation

Scanning electron microscopy (SEM) images were captured using a field-emission microscope (Sirion, FEI, Portland, OR) operated at acceleration voltages 5 to 30 kV. Transmission electron microscopy (TEM) images were taken using a Phillips EM-430 machine operated at 200 kV. The samples were prepared by placing one drop of the alcohol suspension on a silicon substrate or TEM grid, and letting the solvent evaporate slowly in a fume hood. X-ray diffraction (XRD) data were collected from powder samples using a Philips PW1710 diffractometer (with CuK_α radiation, λ = 1.54056 Å) at a scanning rate of 0.02° s^{-1} for 2θ in the range from 10 to 70°. Thermogravimetric analysis (TGA) measurements were performed on a TGA-50/50H Analyzer (Shimadzu, Kyoto, Japan) with a heating rate of 20 °C min^{-1} under a flow of nitrogen gas. Solid state ^{13}C-NMR spectra were taken using a 360 MHz custom-built Spectrometer (Spectral Data Services, Champaign, IL). FT-IR spectra were acquired under ambient conditions using a 1720 Fourier Transform Infrared Spectrophotometer (Perkin-Elmer, Norwalk, CT) with a resolution of 0.5 cm^{-1}.

III. Results and discussion

Nanowires of titania

Titania (TiO_2) is an important oxide, and has been actively explored for use as photocatalysts,[13] supports for catalysts,[14] paper whiteners,[15] functional components in gas (or humidity) sensors and solar cells,[16] and optical coating materials.[17] Titania nanostructures with 1D morphology are particularly interesting for these applications because they might exhibit much higher surface areas than the powder form. As a result, the rate of a reaction on their surfaces could be greatly enhanced. For example, Martin and co-workers have synthesized TiO_2 fibers with a calculated surface area of 315 cm^2 per cm^2 of planar geometric area. It is expected that the decomposition rate of organic molecules on their surface can, in principle, be increased by 315 times as compared with TiO_2 catalysts based on thin films.[18] To this end, a variety of chemical methods have been demonstrated for generating 1D nanostructures of TiO_2 in recent years.[19] Most of them involved the use of hydrothermal (or solvothermal) processes under elevated pressures and temperatures. In comparison, the present method could be performed under the ambient pressure and with conventional glassware.

Electron microscopy and diffraction were used to characterize the change in morphology, microstructure and crystallinity

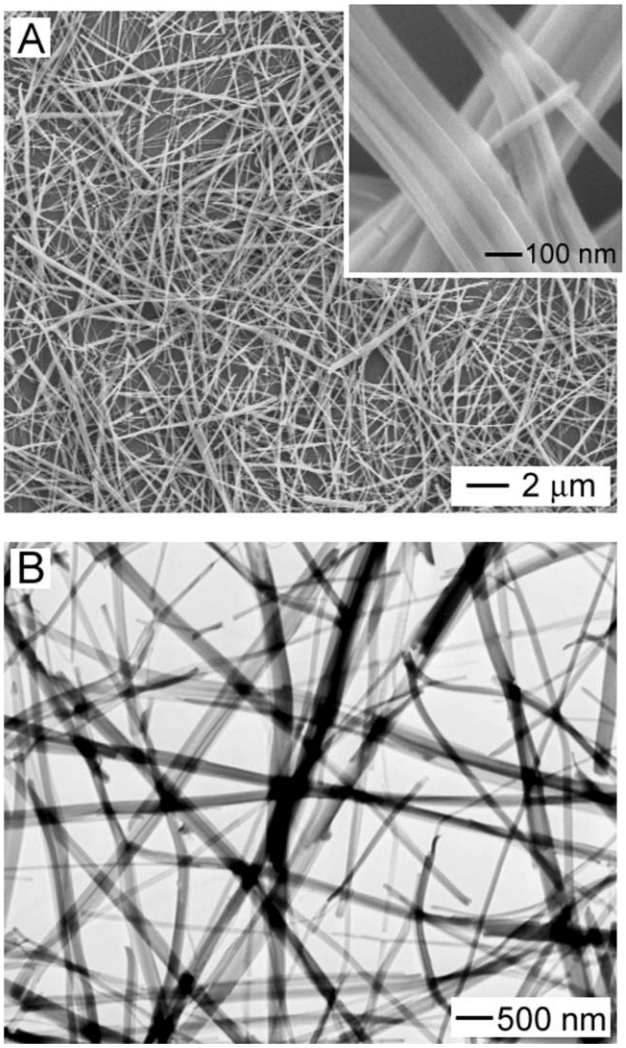

Fig. 1 (A) SEM and (B) TEM images of titanium glycolate nanowires that were synthesized by heating an alkoxide precursor in ethylene glycol at 170 °C for 2 h. The inset shows a blow-up SEM image of the sample, indicating the aggregation of some nanowires into bundles.

associated with calcination of nanowires. Fig. 1 shows SEM and TEM images of titanium glycolate nanowires that were synthesized by adding the alkoxide precursor to ethylene glycol, followed by heating at 170 °C. A closer examination by SEM and TEM indicates that some of the nanowires might have aggregated into bundles and thus appeared thicker than expected when viewed under SEM at relatively low magnifications. Based on the inset of Fig. 1A, the diameters of these nanowires were reasonably uniform, with an average value around 50 ± 8 nm. It was also found the mean diameter of nanowires obtained in each run of synthesis had a strong dependence on the concentration of the precursor solution. When the concentration was higher than 0.02 M, much thicker and shorter nanowires (*i.e.*, rods) were generated, with typical diameters in the range of 1 to 5 μm. Figs. 2A and 2B show SEM and TEM images of the sample same as in Fig. 1, after it had been calcined in air at 500 °C for 2 h. These images confirm that the wire-like morphology was essentially preserved in the calcination process. Fig. 2A also clearly indicates that wires appeared to be several hundred nanometers in diameter were actually bundles of smaller nanowires with diameters ~50 nm. Fig. 2C shows a TEM image of the nanowires after they had been further calcined at 850 °C for 2 h. An obvious change is that the relatively smooth surfaces of the nanowires (up till 500 °C) had been significantly roughened. This could be attributed to the phase transformation from anatase (500 °C) to rutile (850 °C), as well as the growth of crystallites at higher annealing temperatures. These changes in structure and phase were also confirmed by the SAED (see the insets of Figs. 2B and 2C) and XRD (Fig. 2D) patterns. The samples obtained by calcination at 350, 500, and 850 °C could be assigned to the amorphous, anatase (JCPDS File No. 21–1272), and rutile phase (JCPDS File No. 21–1276) of titania, respectively.

The compositional and structural changes associated with the calcination process were also followed using thermogravimetric analysis (TGA) and FT-IR spectroscopy methods. The initial samples were prepared by drying in a vacuum oven at 50 °C for 4 h. Fig. 3A shows the TGA curve recorded under a flow of nitrogen gas, indicating a two-step pattern for weight loss in the temperature range of 25 to 200 °C and 200 to 350 °C, respectively. The first weight loss could be attributed to the desorption of physically adsorbed water and ethylene glycol molecules, and the second one could be ascribed to the removal of ethylene glycol units and the degradation of organic groups contained in the precursor nanowires.[20] Typically, we observed a weight loss of ~3.5% for the first step and ~36.2% for the second step (which correlates well with the ethylene glycol units chemically bonded to titanium in the precursor complex). Fig. 3B shows FT-IR spectra recorded from nanowires that had been calcined at various temperatures up to 500 °C. As the temperature was increased, the peaks corresponding to physically absorbed water or ethylene glycol (the O–H stretching mode at ~3400 cm^{-1} and the O–H bending mode at ~1640 cm^{-1}) were gradually reduced in intensity until they all disappeared around 350 °C. At this temperature, only the Ti–O stretching band still remained at ~640 cm^{-1}, indicating the formation of amorphous TiO_2. Once the amorphous structure had been transformed into the anatase phase of titania at 500 °C, the Ti–O stretching band was shifted to ~465 cm^{-1}. These observations were consistent with previous studies, where conventional alkoxides were used to as sol-gel precursors to prepare various phases of titania.[21]

Nanowires of tin dioxide

Tin dioxide (SnO_2) is another important semiconductor that is widely used in fabricating solar cells, gas (or humidity) sensors, and optical coatings.[22] For examples, fluorine-doped SnO_2 is often applied as coatings on architectural glasses due to its low emissivity of heat or infrared light.[22e] Tin dioxide nanoparticles are considered as one the most important sensing materials for detecting leakage of several types of combustible gases because of their superior sensitivity.[22f] Rutile-phased SnO_2 has been prepared as 1D nanostructures (wires, fibers and belts) by various methods that include electrochemical deposition in an anodic alumina membrane (followed by annealing at elevated temperatures),[23] thermal decomposition (~800 °C) of $SnCl_4 \cdot 5H_2O$ in a melt salt (NaCl),[24] self-catalytic VLS growth,[7a] thermal evaporation[7b–c] and gas-phase, catalytic reaction.[7d–h] No solution-phase method has been demonstrated for producing 1D nanostructures consisting of tin dioxide.

When tin oxalate was added to EG and refluxed at 195 °C, white precipitate would start to appear in the reaction mixture after 2 h. This solid could be readily collected by centrifugation once the solution had been cooled down to room temperature. Fig. 4A shows the SEM image of a typical example, which contained uniform nanowires with a mean diameter around 50 nm and lengths up to ~30 μm. After these nanowires had been heated in air at 500 °C for 2 h, they could be effectively converted to the rutile-phased SnO_2 without altering their 1D morphology. Fig. 4B shows an SEM image of the calcined nanowires, implying that no major change in morphology and dimension occurred in the calcination process. However, both SEM (inset of Fig. 4B) and TEM (Fig. 4C) images at relatively high magnifications revealed that each wire had been transformed from a dense structure (enclosed by a smooth

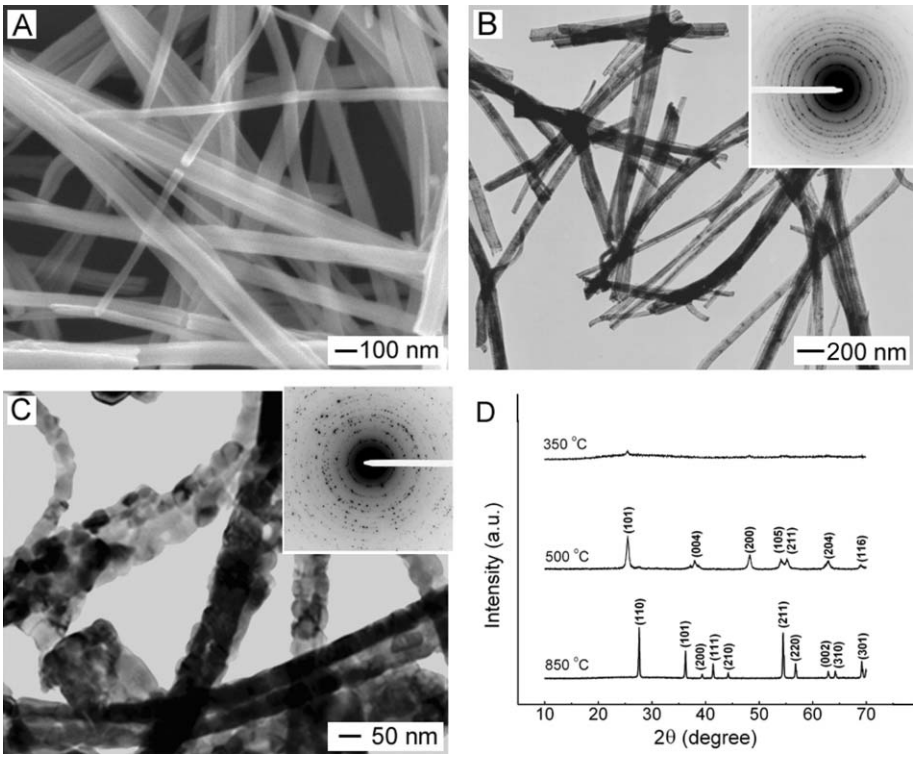

Fig. 2 (A) SEM and (B) TEM images of nanowires after the sample shown in Fig. 1 had been calcined in air at 500 °C for 2 h. The inset shows an SAED pattern of the nanowires, indicating the formation of anatase TiO_2. (C) A TEM image of the same sample after it had been further calcined in air at 850 °C for 2 h. The SAED pattern shown as the inset implies the formation of a pure rutile phase. (D) XRD patterns that confirm the formation of different phases of titania at various calcination temperatures: amorphous (350 °C), anatase (500 °C), and rutile (850 °C).

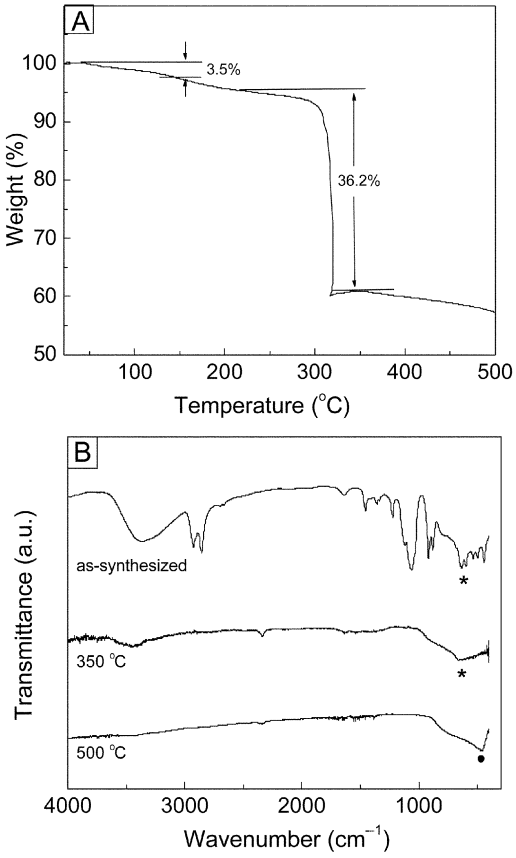

Fig. 3 (A) TGA curve showing the loss of weight for the as-synthesized nanowires of titanium glycolate. (B) FT-IR spectra that were obtained from nanowire samples prepared at different temperatures: titanium glycolate (as-synthesized), amorphous TiO_2 (350 °C) and anatase TiO_2 (500 °C). The star and solid circle denote the Ti–O stretching band associated with the glycolate precursor or amorphous TiO_2 (at ~640 cm^{-1}) and anatase TiO_2 (at ~465 cm^{-1}), respectively.

surface) into a highly porous one consisting of interconnected nanocrystallites. Selected-area electron diffraction (SAED) pattern (not shown here, see ref. 6) confirmed that the nanocrystallites were purely made of the rutile- phased SnO_2. Fig. 4D shows a typical XRD pattern obtained from the calcined nanowires, from which an averaged grain size of ~5 nm was estimated from the width of diffraction peaks using the Scherrer's formula. Both SAED and XRD results suggested that the as-synthesized nanowires were highly crystalline in structure. It is also worth mentioning that the caclcined nanowires were robust enough to be redispersed in water (with brief sonication) and used for further characterization or device fabrication.

Nanowires of indium and lead oxides

Indium oxide (In_2O_3) is an important component for generating conductive transparent substrates such as tin-doped indium oxide (or ITO).[22] This material is crucial to the fabrication of flat panel displays and solar cells owing to its high optical transparency and good electrical conductivity.[22e] Recently, cubic-phased In_2O_3 has been synthesized as 1D nanostructures (wires and belts) using a number of gas-phase methods.[7e] It has also been reported that the metastable, hexagonal phase of In_2O_3 could be prepared as nanowires from InOOH precursors at 490 °C and under ambient pressure.[25] For lead oxides (including PbO, Pb_2O, PbO_2, and Pb_3O_4), they have been employed in many industrial applications because of their distinctive properties. For examples, PbO_2 and Pb_3O_4 are commonly used as electrode materials for batteries.[26] In particular, Pb_3O_4 is attractive as a mixed valence material that often exhibits a unique electronic structure.[27] Single-crystalline nanorods of PbO_2 and Pb_3O_4 have been synthesized in the solution phase with the assistance of surfactants.[28] Nanobelts of β-PbO_2 has been prepared by evaporating PbO powders at 950 °C.[29] Here the polyol-mediated method has also

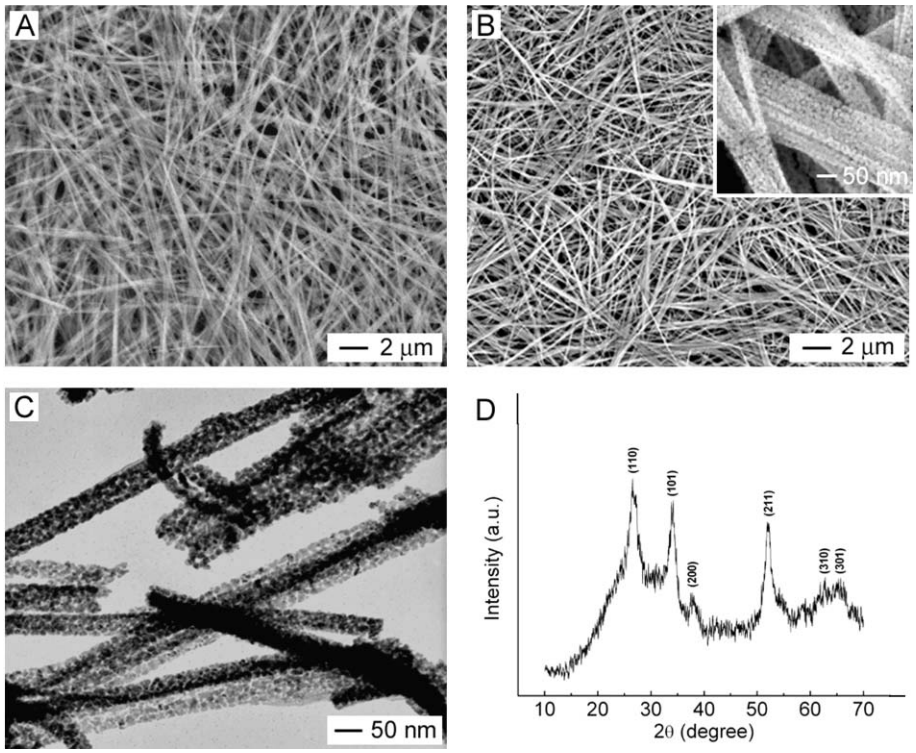

Fig. 4 (A) SEM images of tin glycolate nanowires that were synthesized by refluxing tin oxalate in ethylene glycol at 195 °C for 3 h. (B) SEM and (C) TEM images of SnO_2 nanowires obtained by calcining the precursor sample at 500 °C for 2 h. (D) XRD pattern taken from the same batch of SnO_2 nanowires.

been extended to synthesize In_2O_3 and PbO nanowires with a polycrystalline and highly porous structure.

Fig. 5A shows an SEM image of indium glycolate nanowires that were prepared by replacing $SnC_2O_4{\cdot}2H_2O$ with $In(OOC\text{-}C_7H_{15})(O^iPr)_2$ (as a dispersion in isopropanol). Fig. 5B shows SEM images (at two different magnifications) of the same sample after calcination. In comparison with the SnO_2 nanowires shown in Figs. 4B and 4C, a similar porous structure was also observed for the In_2O_3 nanowires (Fig. 5B). TEM studies (Fig. 5C) indicated that each nanowire was composed of interconnected crystallites with dimensions on the scale of 20 nm. Powder XRD pattern (Fig. 5D) suggested that the as-synthesized wires were highly crystalline in structure, and made of pure In_2O_3. Similar changes in structure and

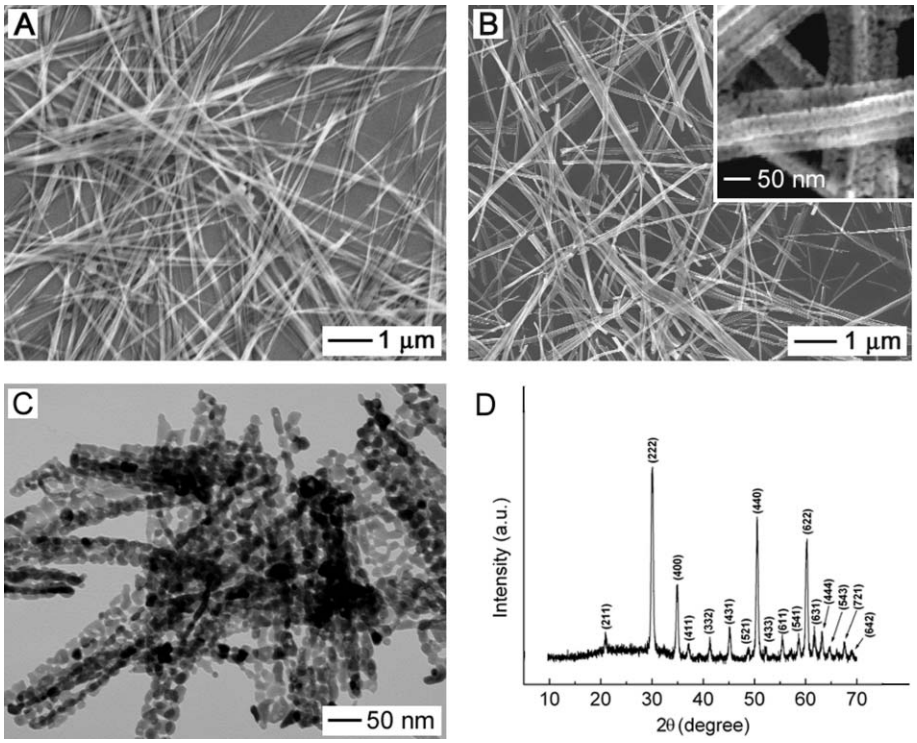

Fig. 5 (A) SEM image of indium glycolate nanowires that were prepared by heating a precursor in ethylene at 170 °C for 2 h. (B) SEM and (C) TEM images of In_2O_3 nanowires generated by calcining the sample in air at 500 °C for 2 h. (D) XRD pattern taken from the same batch of In_2O_3 nanowires.

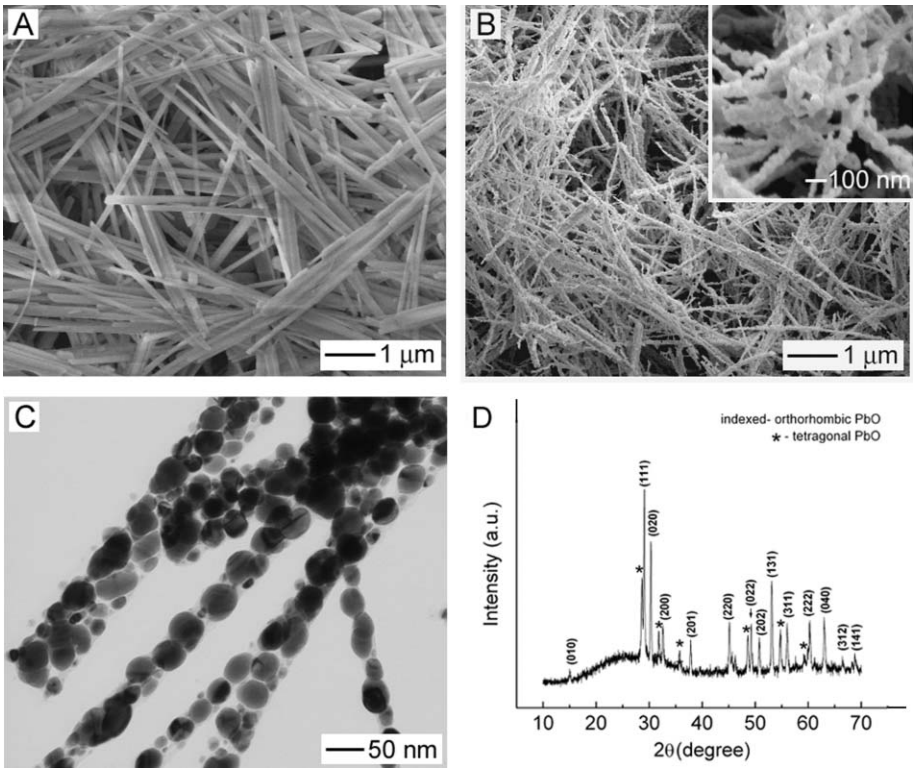

Fig. 6 (A) SEM image of lead glycolate nanowires that were synthesized by heating lead acetate in ethylene glycol at 170 °C for 2 h. (B) SEM and (C) TEM images of PbO nanowires that were obtained by calcining the sample at 600 °C for 4 h. (D) XRD pattern taken from the same batch of PbO nanowires.

morphology were also observed and confirmed by SEM (Figs. 6A and 6B) and TEM (Fig. 6C) studies when $SnC_2O_4{\cdot}2H_2O$ was replaced with $Pb(CH_3COO)_2$. In this case, lead glycolates were formed, which further aggregated into nanostructures having 1D morphology (Fig. 6A). After the sample had been calcined at 600 °C for 4 h, the nanowires had been transformed into chains of crystalline nanoparticles with diameters between 20 and 50 nm. The XRD pattern shown in Fig. 6D suggested that the lead glycolate nanowires had been converted to a mixture of orthorhombic and tetragonal PbO. Note that all the nanowires synthesized using this precursor method share one thing in common: a polycrystalline and highly porous nanostructure made of interconnected nanocrystallites after calcination at elevated temperatures. The nanoparticles within each type of nanowire could be different in size. These porous nanostructures with high surface areas are potentially useful as catalysts (or the supports for catalysts), and may serve as active components in fabricating gas sensors.

The plausible growth mechanism

A number of groups have examined the use of strong complexing agents such as polyols to lower the hydrolysis rates of transition metal alkoxides.[30] Yamamoto and co-workers utilized glycol (primarily ethylene glycol) chelates to control the hydrolysis and polycondensation rates of tin alkoxides.[31] By applying Monte Carlo simulation to study the hydrolysis and condensation of $Sn(O^nBu)_4$, Murakami and co-workers concluded that the glycol could sufficiently suppress the hydrolysis of tin alkoxide due to the formation of linear polymers with relatively high molecular weights in the solution.[32] Unfortunately, no spectroscopic or microscopy analysis of the final products was performed in all these studies. Here we found that glycols could serve as a ligand to form chain-like coordination complexes with Ti(IV), Sn(II), In(III), and Pb(II) cations upon heating. Differently from metal alkoxides (*e.g.*, Ti and In) that are highly susceptible to moisture (white precipitate was immediately formed when it was exposed to air), the glycolate complexes are more resistant to hydrolysis, and could be kept in air for several months without observing any precipitation in the solution system. As the chain-like complexes became sufficiently long, they would aggregate into bundles and then precipitate out from the reaction medium in the form of uniform nanowires (made of the glycolate precursor).

Fig. 7A outlines a plausible mechanism responsible for the formation of SnO_2 nanowires in an isotropic medium.[6] The key

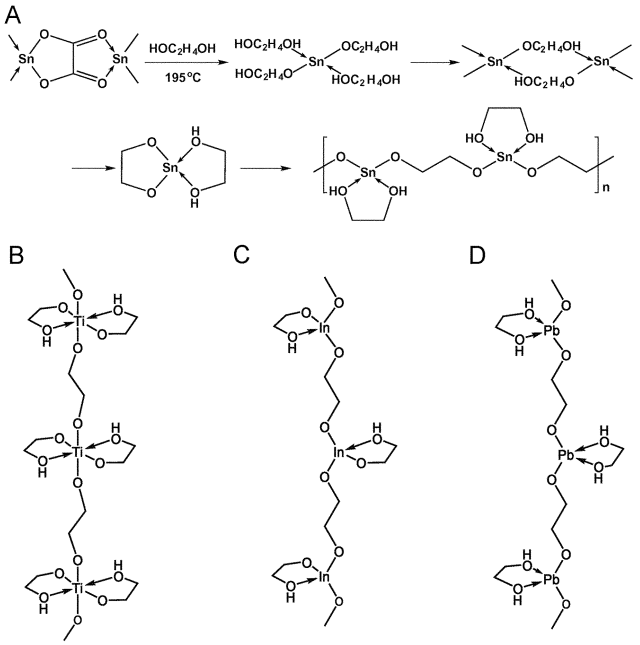

Fig. 7 Schematic illustrations of linear complexes that were formed between ethylene glycol and (A) tin, (B) titanium, (C) indium, and (D) lead cations. These chain-like complexes could further aggregate into nanostructures with 1D morphology due to a weaker interaction (van der Waals force) between chains relative to the interaction between atoms with each chain.

step was the polymerization of tin glycolates, a process that has been discussed in a number of publications for the same or similar metal alkoxides.[33] In their investigation on the reaction between Tin(II) species and ethylene glycol,[33a] Zuckerman *et al.* found that $(O–CH_2CH_2–O–Sn)_n$ was the major component of their product, which shared a white color and insolubility similar to what we observed for our precursor nanowires. Similar polymeric structures were also obtained for the reactions between Tin(II) with other dithiol or diol reagents.[33a,b] In studying another group IV element, Ge, Korb *et al.* also found that a similar repeating unit, $(O–CH_2CH_2–O–Ge)$, existed in their final product for the reaction between GeR_2 and ethylene glycol.[33d] As it has been discussed in all these studies (in particular, the work by Pommier *et al.* on tin glycolate compounds),[33e,f] several intermediate compounds (such as those shown in Fig. 7A) had been identified and characterized with good solubility in benzene. Based on the similarities between our reaction and those reported in the literature, and the observation of a wire-like morphology for the precipitates, we believe they could share similar polymeric chains as the building blocks.

For the synthesis of SnO_2 nanowires, the oxalate groups of SnC_2O_4 were substituted (in the initial stage of refluxing) by ethylene glycol units through the formation of Sn–O– covalent and Sn←OH coordination bonds. This hypothesis was supported by FT-IR measurements, where we observed the disappearance of O–C=O vibrational bands (from oxalate group) and the appearance of CH_2– and C–OH bands (from ethylene glycol unit).[6] As reaction proceeded, the tin glycolates underwent several steps of reactions (as illustrated in the scheme) and eventually formed relatively long chains, which further self-assembled into nanowires. X-ray photoelectron spectroscopic (XPS) studies indicated the oxidation state of tin remained as +2 in the precursor nanowires. Although the nanowires were not soluble in all solvents we have tested, the supernatant solution was found to contain several dimeric and even tetrameric fragments from their mass spectra.[6] From TGA analysis (similar to Fig. 3A), we observed a total of ~36% weight loss around 325 °C under N_2, which is close to the calculated value of 37.5% by considering the loss of two coordinated ethylene glycol and four carbon atoms (in the form of ethylene) for each repeating unit. Figs. 7B–7D show schematic drawings of the proposed structures for linear, polymeric precursors that were involved in the formation of TiO_2, In_2O_3, and PbO nanowires.

Fig. 8 shows solid-state ^{13}C-NMR spectra that we have obtained from nanowires made of glycolate precursors to tin and titanium dioxides. For the tin system, only one relatively broad peak was observed at ~62.8 ppm. According to a recent

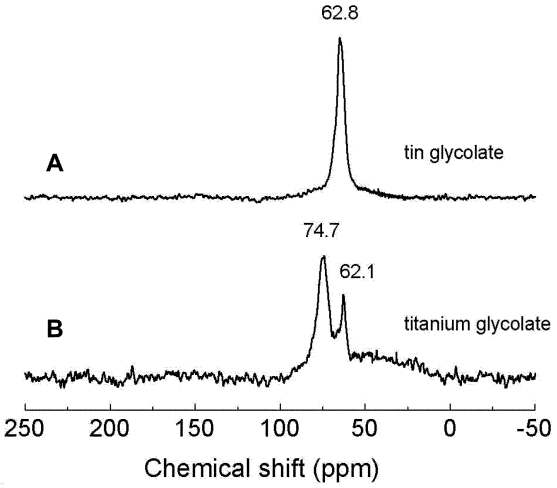

Fig. 8 Solid state ^{13}C-NMR spectra that were taken from precursor nanowires composed of (A) tin(II) and (B) titanium(IV) glycolate complexes.

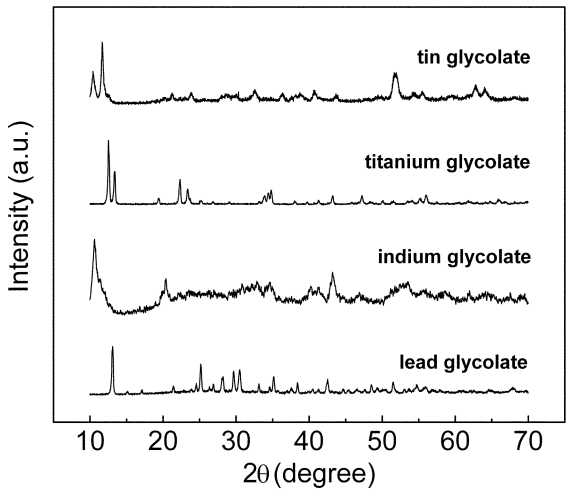

Fig. 9 Powder XRD patterns that were taken from nanowires consisting of tin(II), titanium(IV), indium(III), and lead(II) glycolate complexes. Note the appearance of sharp diffraction peak(s) in the low-angle region.

solid-state NMR study on tin glycolates, the chemical shift for C atoms in the moiety of –C–O–Sn was located at ~61.5 ppm,[12a,34] a value similar to what we observed here. In fact, for C atoms in free ethylene glycol and those bonded directly to oxygen in many other polymeric species,[34] their chemical shifts were all located in the range of 60–65 ppm. According to these studies, the difference in chemical shift for the C atoms in the covalently bonded ethylene glycol unit and the C atoms in the coordinated ethylene glycol ligand should be minor for the polymeric structure described in Fig. 7A. The relatively broad peak we obtained here could be attributed to the overlapping between the two peaks of C atoms in these two different ethylene glycol moieties. In the titanium precursor (Fig. 8B), the difference between carbon atoms in the backbone and side chain was significant enough that two well-resolved peaks were detected around 62.1 and 74.7 ppm.

Fig. 9 shows some typical XRD patterns that were taken from the metal (Sn, Ti, In, and Pb) glycolate nanowires. These patterns exhibit a striking similarity in the emergence of diffraction peaks, especially those located at low angles. This similarity could be attributed to the similar way of packing for the linear building blocks associated with these precursor wires. Because these metals have different oxidations states and bonding configurations, it is understandable that their crystallographic structures (and thus the diffraction patterns) could be slightly different.[35] The exact crystal structure of each type of precursor nanowire is yet to be determined. For the linear chains of tin glycolate shown in Fig. 7A, the repeating unit was found to have the following dimensions ($a \approx 10$ Å, $b \approx 3.6$ Å, and $c \approx 15$ Å) by structural modeling (CHEM 3D® Ultra 8.0, CambridgeSoft). If the crystal lattice is assumed to be orthorhombic (with its constants being the same as the dimensions estimated for the repeating unit) the peak positions calculated using the ENDEAVOUR (Version 1.2, Crystal Impact GbR) program were in reasonable agreement with the experimental data.[6] The XRD patterns shown here indicate that a similar mechanism was also shared by the systems that led to the formation of TiO_2, In_2O_3, and PbO nanowires. Due to the fact that we could not find any solvent to dissolve the nanowires made of these glycolate precursors, we believed that these complexes might also exist as relatively long-chain polymers.

Application of SnO_2 nanowires in gas sensing

As an *n*-type semiconductor, SnO_2 has been actively explored as the functional component in detecting combustible gases such as CO, H_2, and CH_4.[36] Most of these studies have concentrated on devices that were fabricated with polycrystalline films (consisting of small SnO_2 particles) as the sensing units.[37] Recent work

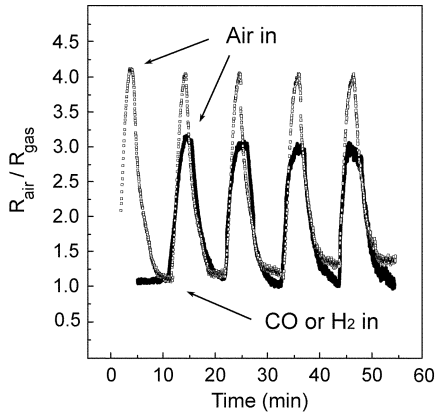

Fig. 10 Change in resistance for a sensor based on the polycrystalline SnO_2 nanowires, when the surrounding gas was switched between air and 20 ppm CO (dashed curve) or 500 ppm H_2 (solid curve) under ambient conditions.

indicated that single crystalline nanobelts of SnO_2 could also be employed to fabricate nanoscale sensors for the detection of various gases or vapors.[38] As limited by the relatively small surface areas of these nanostructures, high sensitivity and reversibility could only be achieved at an elevated temperature or by exposure to UV light. As prompted by their porous appearance, we suspected that the polycrystalline nanowires of SnO_2 prepared using the present approach should be particularly useful as the functional component in fabricating gas sensors. As a matter of fact, the polycrystalline SnO_2 nanowires were found to exhibit both enhanced sensitivity and reversibility under ambient conditions.[6] Fig. 10 shows the changes in resistance measured at room temperature when a thin-film-based sensor was exposed to 20 ppm CO and 500 ppm H_2, respectively. In comparison, we observed an at least 8000-fold change in resistance between the on and off stages for the saturated vapor of ethanol ($\sim$6%, $V_{ethanol}/V_{air}$). For CO and H_2, similar change were also observed, albeit the magnitude of change was reduced to $\sim$3 for H_2 and $\sim$4 for CO due to the relatively low concentrations of these gases. It is also worth noting that such on- and off-responses could be repeated at least 10 times without observing any drop in the signal amplitude. As a control experiment, we monitored the change in resistance for the sensor over a period of 24 hours (Fig. 11A). In this case, the sensor was kept in the closed plastic tube specially designed to host the sensing unit. The results indicate that the resistance was stable as long as the environment around the sensor did not change since SnO_2-based sensors are also known to be sensitive to humidity.[37c] We also compared the resistance of the sensor when it was exposed to air with different levels of humidity (Fig. 11B). In this demonstration, we simply exposed the sensor to the air of an ordinary laboratory and the air of a fume hood. With the use of a hygrometer, the humidity of these two locations was 65% and 15%, respectively. The resistance was also different by as much as 20 times. The results also suggest the potential use of our SnO_2 nanowires in applications for humidity sensing.

For SnO_2-based sensors, the change in resistance is believed to be a result of the adsorption and desorption of gas molecules on the surface of a functional component. In almost all previous studies, elevated temperatures or UV light had to be utilized to improve the molecular desorption kinetics and thus to help "clean" the surface.[37,38] For the sensors described here, we believe that the high sensitivity and reversibility under ambient conditions originated from the intrinsically small grain size and high surface-to-volume ratios associated with the polycrystalline oxide nanowires.[39] For conventional, film-type sensors based on small particles of SnO_2, the surface-to-volume ratio is relatively low as a result of large grain sizes ($\sim$200 nm). Furthermore, only a very thin layer of the film close to the surface can be activated

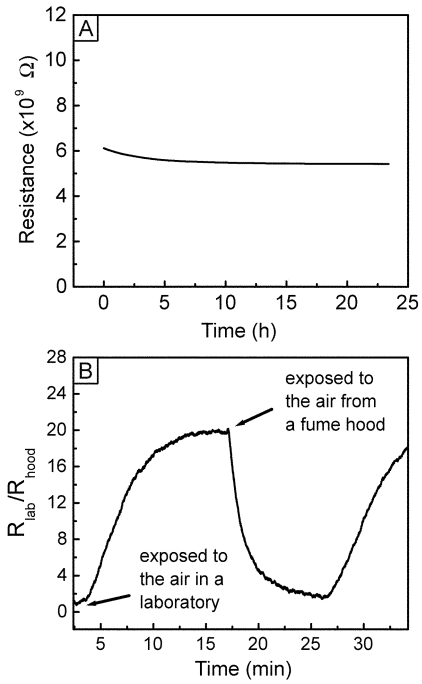

Fig. 11 (A) Change in resistance for a sensor kept in the closed plastic tube over a period of 24 hours. (B) Variation in resistance when the sensor was exposed to the air in an ordinary lab and to the air in a fume hood, respectively. The change was mainly caused by the difference in humidity.

during gas detection due to the dense structure of a compact film. In comparison, there exists a network of interconnected pores in our nanowire-based films, where the SnO_2 nanowires are randomly oriented to generate a highly porous structure. The interconnected network of pores permits both the target species and the background gas to access all the surfaces of SnO_2 nanowires contained in the sensing film. Different from sensors made of single crystalline SnO_2 nanobelts, the small grains of SnO_2 in our nanowires also allowed the sensors to be operated in the most sensitive, grain-controlled mode. As shown by simulation, the sensitivity could be exponentially enhanced when the grain size is reduced to a scale comparable to the space-charge length (for SnO_2, this value is $\sim$6 nm).[6] Last but not least, the operation of such sensors at room temperature also helps to eliminate grain size changes that might occur as a result of thermal-induced sintering effect.

IV. Conclusion

We have demonstrated a generic approach to the large-scale synthesis of metal oxide nanowires with polycrystalline and thus porous structures. The key to the success of this synthesis was the use of ethylene glycol to form chain-like complexes with appropriate metal cations, which could readily aggregate into 1D nanostructures within an isotropic medium. The immediate product of such a synthesis was nanowires made of the metal glycolate that could be further converted to a metal oxide by calcination in air at elevated temperatures. For example, the titanium glycolate could be transformed into the amorphous phase of TiO_2 at 350 °C, the anatase phase at 500 °C, and the rutile phase at 850 °C. This polyol-mediated method provides a number of attractive features when compared with the gas-phase approach, including a larger scale of production, as well as the formation of nanostructures with higher porosity and thus larger surface areas. It is believed that this approach could also be extended to process many other functional oxides (*e.g.*, ZnO, NiO, and ZrO_2) as polycrystalline 1D nanostructures.

Acknowledgements

This work has been supported in part by an AFOSR-MURI grant awarded to the UW, a Career Award from the NSF (DMR-9983893), and a Fellowship from the David and Lucile Packard Foundation. Y. X. is an Alfred P. Sloan Research Fellow (2000) and a Camille Dreyfus Teacher Scholar (2002). T. H. thanks the Center for Nanotechnology at the UW for an IGERT Fellowship supported by the NSF (DGE-9987620). We thank Dr L.-Q. Wang at PNNL for her help with solid ^{13}C-NMR studies.

References

1 For a recent review, see: Y. Xia, P. Yang, Y. Sun, Y. Wu, B. Mayers, B. Gates, Y. Yin, F. Kim and H. Yan, *Adv. Mater.*, 2003, **15**, 353.
2 W. Noll, *Z. Anorg. Allg. Chem.*, 1950, **261**, 1.
3 (*a*) J. J. Stejny, R. W. Trinder and J. Dlugosz, *J. Mater. Sci.*, 1981, **16**, 3161; (*b*) J. J. Stejny, J. Dlugosz and A. Keller, *J. Mater. Sci.*, 1979, **14**, 1291.
4 (*a*) J. M. Tarascon, F. J. DiSalvo, C. H. Chen, P. J. Carrol, M. Walsh and L. Rupp, *J. Solid State Chem.*, 1985, **58**, 290; (*b*) P. Davidson, J. C. Gabriel, A. M. Levelut and P. Batail, *Europhys. Lett.*, 1993, **21**, 317; (*c*) B. Messer, J. H. Song, M. Huang, Y. Wu, F. Kim and P. Yang, *Adv. Mater.*, 2000, **12**, 1526.
5 (*a*) B. Mayers, K. Liu, D. Sunderland and Y. Xia, *Chem. Mater.*, 2003, **15**, 3852; (*b*) B. Mayers, B. Gates and Y. Xia, *Int. J. Nanotechnol.*, 2003, **1**(2), 89; (*c*) B. Gates, B. Mayers, A. Grossman and Y. Xia, *Adv. Mater.*, 2002, **14**, 1749; (*d*) B. Mayers and Y. Xia, *J. Mater. Chem.*, 2002, **12**, 1875; (*e*) B. Mayers and Y. Xia, *Adv. Mater.*, 2002, **14**, 279; (*f*) B. Gates, B. Mayers, B. Cattle and Y. Xia, *Adv. Funct. Mater.*, 2002, **12**, 219; (*g*) B. Mayers, B. Gates, Y. Yin and Y. Xia, *Adv. Mater.*, 2001, **13**, 1380; (*h*) B. Gates, Y. Yin and Y. Xia, *J. Am. Chem. Soc.*, 2000, **122**, 12582.
6 Y. Wang, X. Jiang and Y. Xia, *J. Am. Chem. Soc.*, 2003, **125**, 16176.
7 (*a*) Z. R. Dai, Z. W. Pan and Z. L. Wang, *Adv. Funct. Mater.*, 2003, **13**, 9; (*b*) Y. Chen, X. Cui, K. Zhang, D. Pan, S. Zhang, B. Wang and J. G. Hou, *Chem. Phys. Lett.*, 2003, **369**, 16; (*c*) Z. Dai, J. L. Gole, J. D. Stout and Z. Wang, *J. Phys. Chem. B*, 2002, **106**, 1274; (*d*) J. K. Jian, X. L. Chen, W. J. Wang, L. Dai and Y. P. Xu, *Appl. Phys. A*, 2003, **76**, 291; (*e*) C. Li, D. H. Zhang, S. Han, X. L. Liu, T. Tang and C. W. Zhou, *Adv. Mater.*, 2003, **15**, 143; (*f*) C. Liang, G. Meng, Y. Lei, F. Phillipp and L. Zhang, *Adv. Mater.*, 2001, **13**, 1330; (*g*) P. Nguyen, H. T. Ng, J. Kong, A. M. Cassell, R. Quinn, J. Li, J. Han, M. McNeil and M. Meyyappan, *Nano Lett.*, 2003, **3**, 925; (*h*) X. Peng, G. Meng, X. Wang, Y. Wang, J. Zhang, X. Liu and L. Zhang, *Chem. Mater.*, 2002, **14**, 4490.
8 (*a*) Y. Sun, Y. Yin, B. Mayers, T. Herricks and Y. Xia, *Chem. Mater.*, 2002, **14**, 4736; (*b*) Y. Sun and Y. Xia, *Science*, 2002, **298**, 2176; (*c*) Y. Sun, Y. Yin, B. Mayers, T. Herricks and Y. Xia, *Chem. Mater.*, 2002, **14**, 4736; (*d*) Y. Sun and Y. Xia, *Analyst*, 2003, **128**, 686; (*e*) Y. Sun and Y. Xia, *Adv. Mater.*, 2003, **15**, 695; (*f*) Y. Sun, B. Mayers and Y. Xia, *Adv. Mater.*, 2003, **15**, 641; (*g*) Y. Sun, B. Mayers and Y. Xia, *Nano Lett.*, 2003, **3**, 675; (*h*) Y. Sun, B. Mayers, T. Herricks and Y. Xia, *Nano Lett.*, 2003, **3**, 955; (*i*) P. Toneguzzo, G. Viau, O. Acher, F. Fievet-Vincent and F. Fievet, *Adv. Mater.*, 1998, **10**, 1032; (*j*) L. K. Kurihara, G. M. Chow and P. E. Schoen, *Nanostruct. Mater.*, 1995, **5**, 607; (*k*) F. Fievet, J. P. Lagier and B. Blin, *Solid State Ionics*, 1989, **32-3**, 198; (*l*) S. Ammar, A. Helfen, N. Jouini, F. Fievet, I. Rosenman, F. Villain, P. Molinie and M. Danot, *J. Mater. Chem.*, 2001, **11**, 186.
9 T. C. Mo and S. Y. Chen, *Ferroelectrics*, 2001, **259**, 305.
10 S. J. Lee, M. D. Biegalski and W. M. Kriven, *J. Mater. Res.*, 1999, **14**, 3001.
11 M. Kakihana, M. Arima, M. Yoshimura, N. Ikeda and Y. Sugitani, *J. Alloy Compd.*, 1999, **283**, 102.
12 (*a*) R. W. J. Scott, N. Coombs and G. A. Ozin, *J. Mater. Chem.*, 2003, **13**, 969; (*b*) D. Khushalani, G. A. Ozin and A. Kuperman, *J. Mater. Chem.*, 1999, **9**, 1483; (*c*) D. Khushalani, G. A. Ozin and A. Kuperman, *J. Mater. Chem.*, 1999, **9**, 1491.
13 (*a*) G. Dagan and M. Tomkiewicz, *J. Phys. Chem.*, 1993, **97**, 12651; (*b*) M. Anpo, T. Shima, S. Kodama and Y. Kubokawa, *J. Phys. Chem.*, 1987, **91**, 4305; (*c*) R. W. Matthew, *J. Phys. Chem.*, 1987, **91**, 3328.
14 S. Matsuda, *Appl. Catal.*, 1983, **8**, 149.
15 W. P. Hsu, R. C. Yu and E. Matijević, *J. Colloid Interface Sci.*, 1993, **156**, 56.
16 (*a*) A. M. Azad, L. B. Younkman and S. A. Akbar, *J. Am. Ceram. Soc.*, 1994, **77**, 481; (*b*) A. M. Katayama, H. Hasegawa, T. Noda, T. Akiba and H. Yanagida, *Sens. Actuators, B*, 1992, **2**, 143; (*c*) S. Uchida, R. Chiba, M. Tomiha, N. Masaki and M. Shirai, *Electrochem.*, 2002, **70**, 418.
17 G. A. Battiston, R. Gerbasi, M. Porchia and L. Rizzo, *Chem. Vap. Deposition*, 1999, **5**, 73.
18 B. B. Lakshmi, P. K. Dorhout and C. R. Martin, *Chem. Mater.*, 1997, **9**, 896.
19 (*a*) Z.-Y. Yuan, W. Z. Zhou and B.-L. Su, *Chem. Commun.*, 2002, 1202; (*b*) S. Kobayashi, K. Hanabusa, N. Hamasaki, M. Kimura, H. Shirai and S. Shinkai, *Chem. Mater.*, 2000, **12**, 1523.
20 M. Popa and M. Kakihana, *Solid State Ionics*, 2002, **151**, 251.
21 (*a*) K. Nakamoto, *Infrared and Raman Spectra of Inorganic and Coordination Compounds*; Wiley, New York, c1978, p. 220; (*b*) D. C. Bradley, R. C. Mehrotra and D. P. Gaur, *Metal Alkoxides*; Academic Press, New York, 1978, p. 119; (*c*) A. J. Maira, J. M. Coronado, V. Augugliaro, K. L. Yeung, J. C. Conesa and J. Soria, *J. Catal.*, 2001, **202**, 413.
22 (*a*) P. H. Wei, G. B. Li, S. Y. Zhao and L. R. Chen, *J. Electrochem. Soc.*, 1999, **146**, 3536; (*b*) H. S. Varol and A. Hinsch, *Sol. Energy Mater. Sol. Cells*, 1996, **40**, 27; (*c*) T. W. Kim, D. U. Lee and Y. S. Yoon, *Solid State Commun.*, 2000, **115**, 503; (*d*) G. Sberveglieri, G. Faglia, S. Groppli and P. Nelli, *Sens. Actuators, B*, 1992, **5**, 79; (*e*) D. S. Ginley and C. Bright, *Mater. Res. Soc. Bull.*, 2000, **25**, 15; (*f*) N. Yamazoe, *Sens. Actuators, B*, 1991, **5**, 7.
23 (*a*) M. Zheng, G. Li, X. Zhang, S. Huang, Y. Lei and L. Zhang, *Chem. Mater.*, 2001, **13**, 3859; (*b*) H. Cao, X. Qiu, Y. Liang and Q. Zhu, *Appl. Phys. Lett.*, 2003, **83**, 761.
24 W. Wang, C. Xu, G. Wang, Y. Liu and C. Zheng, *J. Appl. Phys.*, 2002, **92**, 2740.
25 D. Yu, S. Yu, S. Zhang, J. Zuo, D. Wang and Y. Qian, *Adv. Funct. Mater.*, 2003, **13**, 497.
26 (*a*) D. Pletcher and F. C. Walsh, *Industrial Electrochemistry*; Chapman and Hall, London, 1990; (*b*) C. Barriga, S. Maffi, L. P. Bicelli and C. Malitesta, *J. Power Sources*, 1991, **34**, 353.
27 H. J. Terpstra, R. A. DeGroot and C. Haas, *J. Phys. Chem. Solids*, 1997, **58**, 561.
28 M. Cao, C. Hu, G. Peng, Y. Qi and E. Wang, *J. Am. Chem. Soc.*, 2003, **125**, 4982.
29 Z. Pan, Z. Dai and Z. Wang, *Appl. Phys. Lett.*, 2002, **80**, 309.
30 (*a*) A. Léaustic, F. Bahonneau and J. Livage, *Chem. Mater.*, 1989, **1**, 248; (*b*) A. Yamamoto and S. Kambara, *J. Am. Chem. Soc.*, 1957, **79**, 4344.
31 O. Yamamoto, T. Sasamoto and M. Inagaki, *J. Mater. Res.*, 1992, **7**, 2488.
32 Y. Murakami, T. Matsumoto, K. Yahikozawa and Y. Takasu, *Catal. Today*, 1995, **23**, 283.
33 (*a*) D. Fenton, R. Gould, P. Harrison, T. Harvey, G. Omietanski, C. Sze and J. Zuckerman, *Inorg. Chim. Acta*, 1970, **4**, 235; (*b*) G. Cocks and J. Zuckerman, *Inorg. Chem.*, 1965, **4**, 592; (*c*) W. Honnick and J. Zuckerman, *Inorg. Chem.*, 1978, **17**, 501; (*d*) G. Korb, G. Levy, M. Brini and A. Deluzarche, *J. Organomet. Chem.*, 1970, **23**, 437; (*e*) J. Pommier and J. Valade, *J. Organomet. Chem.*, 1968, **12**, 433; (*f*) J. Pommier, E. Mendes and J. Valade, *J. Organomet. Chem.*, 1973, **55**, C19; (*g*) Y. Murakami, T. Matsumoto, K. Yahikozawa and Y. Takasu, *Catalysis Today*, 1995, **23**, 383; (*h*) R. Mehrotra and V. Gupta, *J. Organomet. Chem.*, 1965, **4**, 151; (*i*) D. Gaur, G. Srivastava and R. Mehrotra, *J. Organomet. Chem.*, 1973, **47**, 95; (*j*) D. Bradley, R. Mehrotra and D. Gaur, *Metal Alkoxides*; Academic, London, 1978, Chapter 4.
34 (*a*) G. Russell, P. Henrichs, J. Hewitt, H. Grashof and M. Sandhu, *Macromolecules*, 1981, **14**, 1764; (*b*) F. Barroso-Bujans, R. Martinez and P. Ortiz, *J. Appl. Polym. Sci.*, 2003, **88**, 302.
35 D. Bradley, R. Mehrotra and D. Gaur, *Metal Alkoxides*; Academic Press, London, 1978, pp.149–298.
36 J. Watson, *Sens. Actuators*, 1984, **5**, 29.
37 (*a*) R. Scott, S. Yang, D. Williams and G. Ozin, *Chem. Commun.*, 2003, 688; (*b*) P. Camagni, G. Faglia, P. Galinetto, C. Perego, G. Samoggia and G. Sberveglier, *Sens. Actuators, B*, 1996, **31**, 99; (*c*) K. Ihokura and J. Watson, *The Stannic Oxide Gas Sensor*; CRC; Boca Raton, FL, 1994.
38 (*a*) A. Kolmakov, Y. Zhang, G. Cheng and M. Moskovits, *Adv. Mater.*, 2003, **15**, 997; (*b*) M. Law, H. Kind, B. Messer, F. Kim and P. Yang, *Angew. Chem., Int. Ed.*, 2002, **41**, 2405; (*c*) E. Comini, G. Faglia, G. Sberveglieri, Z. Pan and Z. Wang, *Appl. Phys. Lett.*, 2002, **81**, 1869.
39 F. Favier, E. Walter, M. Zach, T. Benter and R. Penner, *Science*, 2001, **293**, 2227.